Uncertainty quantification and sensitivity analysis during the development and validation of numerical artery models

Friederike Schäfer [a,*], Jacob Sturdy [a], Mateusz Mesek [b], Aleksander Sinek [b], Ryszard Białecki [b], Ziemowit Ostrowski [b], Bartłomiej Melka [b], Marcin Nowak [b], Leif Rune Hellevik [a]

[a] *Division of Biomechanics, Department of Structural Engineering, NTNU, Trondheim, Norway,*

[b] Biomedical Engineering Lab, Department of Thermal Technology, SUT, Gliwice, Poland,
friederike.e.schaefer@ntnu.no

Abstract

Increasing age and cardiovascular diseases lead to stiffening of the vasculature. Knowledge about an individual's arterial stiffness gives insights into the current state of the cardiovascular system and it is considered to be a valuable diagnostic index. However, arterial stiffness cannot be measured directly. Numerical modelling based on measurements of flow and deformation in an individual's artery enable an indirect means. Our research aims to develop a method to estimate the local arterial stiffness of an artery from non-invasive measurements through inverse modelling. Experimental measurement limitations and the unmeasurable nature of model input parameters lead to uncertainties in the model prediction. Uncertainty quantification and sensitivity analysis (UQSA) inform about how the model prediction is influenced by these uncertainties. Due to the computational expenses of 3D fluid-structure interaction (FSI) models, we reduced the model's complexity to a 1D model. To verify the 3D-FSI implementation and validate the 1D implementation we performed simulated inflation tests and compared the results with analytical theory. 3D-FSI simulations were performed and compared to the 1D-model predictions for different simplification assumptions. To quantify the impact of uncertainties in input data, polynomial chaos expansion for UQSA was applied to the 1D-model. This analysis revealed the model input parameters which lead to the highest variability in model prediction. UQSA showed that variations in the Young's modulus and the lumen radius lead to the largest variability in the 1D-model prediction. Thus, we focused in the validation process on the comparison between the the arterial wall behaviour between the 1D and the 3D-FSI model.

1. Introduction

Arterial stiffening is an ubiquitous process associated with human ageing and can be observed in all humans over age 30 [1]. Stiffening itself contributes to cardiovascular disease, and some diseases, such as arteriosclerosis, directly cause arterial stiffening [2]. Clinicians recognize arterial stiffness as a valuable biomarker describing the overall state of an individual's cardiovascular system. However, arterial stiffness cannot be measured directly [3]. Using numerical models and an inverse problem formulation, we seek to estimate arterial stiffness from non-invasive flow and deformation measurements.

The accuracy of an inverse problem's solution depends on the accuracy of the forward model response, which is limited by experimental measurement uncertainties and unavailable model parameters. Through uncertainty quantification (UQ), the propagation of input uncertainties through a numerical model can be investigated. Subsequent sensitivity analysis (SA) attributes the uncertainty in the model response to individual model input parameters and their interactions [4]. These results can help to identify key sources of error as well as focus efforts on developing and validating influential portions of the forward model. However, UQSA require the evaluation of the entire uncertain input parameter space increasing the computational expenses with the number of uncertain model parameters and dimensions.

Three-dimensional (3D) models of vessel segments enable the simulation of patient-specific geometries giving spatially resolved insights into a patients' haemodynamics. Of all model types, fluid-structure interaction (FSI) models represent the anatomical and physiological state in the greatest detail. However, the computational expenses for such models are high, making it impractical to conduct several thousand model evaluations for UQSA.

Reducing the spatial model dimension to one (1D) decreases the information which can be retrieved from the model, but it also reduces the computational expenses significantly. In vessel segments where the vascular flow is independent of the geometry, 1D models represent hemodynamic quantities like pressure and flow rate accurately [5]. Low computational expenses and the ability to evaluate specific hemodynamic quantities accurately make 1D models suitable for UQSA.

The aim of this work is to compare the 1D model prediction of pressure, flow rate, and radial deformation of the common carotid artery (CCA) against a 3D-FSI model and to determine focus for model development. To gain insights into the uncertainty propagation from the input parameters to the 1D model response, we applied polynomial chaos (PC) expansion. PC is an efficient way of representing random model inputs as a polynomial function of another random variable enabling

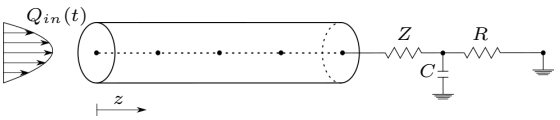

Figure 1: Representation of the 1D-model used in this validation work. As an outlet boundary condition, a Windkessel model with arterial impedance Z, compliance C, and resistance R is applied.

the evaluation of qualitative and quantitative uncertainty measures [6]. Information about the most sensitive 1D model input parameters can be used in the process of validating low-dimensional models against higher fidelity models and experimental measurements.

2. Methodology

In this work, steps for the verification and validation of a 1D-model of the CCA were conducted. The workflow included verification of the 1D-model, UQSA, as well as initial steps for the validation against a 3D-FSI model.

2.1. 1D-model formulation

The CCA in the 1D model is represented as a straight deformable tube, depicted in Fig. 1. The quantities of interest, pressure p, volumetric flow rate Q, and radius change ΔR, are evaluated at five equidistant nodes located on the tube's centreline. In the vessel, laminar and axisymmetric blood flow is assumed. Impermeability and homogeneity characterize the vessel wall. Deformation of the vessel wall is purely in the circumferential direction. Blood is modelled as an incompressible Newtonian fluid. Based on these assumptions, the conservation laws of mass and momentum can be formulated as

$$\frac{\partial A}{\partial t} + \frac{\partial (Au)}{\partial z} = 0 \tag{1a}$$

$$\frac{\partial u}{\partial t} + u\frac{\partial u}{\partial z} + \frac{1}{\rho_f}\frac{\partial p}{\partial z} = \frac{f}{\rho_f A}, \tag{1b}$$

where the quantities u and p are the velocity and pressure averaged over the vessel cross-section A, ρ_f is the fluid density, and f represents the frictional force per unit length [7]. The velocity profile of the fluid flow determines the magnitude of f which accounts for the wall shear stress and convective inertia terms. A commonly used symmetric polynomial model of the velocity is applied:

$$u_r(z,r,t) = u(z,t)\frac{\zeta+2}{\zeta}\left[1-\left(\frac{r}{R}\right)^{\zeta}\right], \tag{2}$$

where u_r is the velocity at a given radial distance r from the centerline. R denotes the vessel radius, and the polynomial order ζ determines the shape of the profile, where a higher ζ corresponds to a blunter profile. For this profile and a constant dynamic blood viscosity μ, the friction term becomes $f = -2(\zeta+2)\mu\pi u$. In all simulations of this work, a parabolic velocity profile with $\zeta = 2$ was applied.

The arterial wall was modelled as a thin, incompressible, homogenous, isotropic, elastic material. The tube law describes the fluid-structure interaction by relating the pressure to the area with

$$\begin{aligned} p &= p_{dia} + \frac{\beta}{A_{dia}}(\sqrt{A} - \sqrt{A_{dia}}) \\ \text{with } \beta &= \frac{\sqrt{\pi}Eh}{(1-\nu^2)}, \end{aligned} \tag{3}$$

where p_{dia} and A_{dia} are the diastolic pressure and cross-sectional area, respectively. Generally, A_{dia} is larger than the reference area A_0 because A_0 is the lumen area when $p = 0$. Material properties of the vessel wall are the Young's modulus E, wall thickness h, and Poisson's ratio ν.

Eqs. 1 resemble a hyperbolic system of equations such that at each boundary one boundary condition (BC) needs to be specified. A representative volumetric flow rate $Q_{in}(t)$ of the CCA was imposed at the inlet boundary [8]. At the outlet, the 1D-model was coupled with a three element Windkessel model, mimicking the behaviour of the downstream vasculature. The elements of the Windkessel model are a resistor Z modelling the arterial impedance, a second resistor representing the peripheral resistance R, and a capacitor C, which mimics the arterial compliance. Relating pressure and flow, the Windkessel model equation reads

$$\frac{\partial p}{\partial t} + \frac{p}{RC} = \left(\frac{1}{C} + \frac{Z}{RC}\right) Q + Z\frac{\partial Q}{\partial t}. \tag{4}$$

As an initial condition, pressure in the entire domain was set to $P_d = 74.5$ mmHg [9] and the initial flow rate was 7.7 mL/s. An explicit MacCormack scheme was used to solve the system of equations. This solution method is second order in space and time. To grant stability of an explicit scheme, the Courant-Friedrich-Lewy (CFL) condition needs to be satisfied. Information travels in the domain from one element to the next with a forward travelling wave, which is the sum of the fluid flow speed u and the pulse wave velocity c. Using the constitutive equation given in Eq. 3, the pulse wave velocity is

$$c = \sqrt{\frac{\beta}{2\rho A_{dia}}} A^{1/4}. \tag{5}$$

The CFL condition becomes with the grid spacing Δx and the time step Δt

$$CFL = (u+c)\frac{\Delta t}{\Delta x} \leq 1. \tag{6}$$

Since Eqs. 1 form a hyperbolic system of equations, physiological conditions have two Riemann invariants that travel in opposite directions, thus at each boundary the BCs can only be specified to determine the single Riemann invariant entering the domain [10]. We imposed a volumetric inflow at the inlet and a relationship between pressure and flow at the outlet.

2.2. Grid independence of the 1D model

Model verification is essential for every numerical study [11]. In this work, a periodic solution of pressure, flow and radius change was reached within twelve cardiac cycles, demonstrating iterative convergence. Consistency of the model was shown through mass conservation over five consecutive heart beats and a pressure drop from inlet to outlet. In total, three grids with increasing number of grid points were tested. The coarsest grid with a total of five nodes returned the same values for pressure, flow, and radius change as the finer grids with ten and 15 nodes. Therefore, all simulations used a grid of five nodes. The maximum allowed time step $\Delta t_{\max}$ during the simulations was determined with a maximal CFL number of 0.8 and the five grid points following Eq. 6. To check temporal convergence, the time step was set manually in two subsequent simulation runs to $0.5\ \Delta t_{\max}$ and $0.25\ \Delta t_{\max}$. Decreasing the time step did not alter the

Table 1: Baseline hemodynamic parameters and uncertainties of the 1D CCA-model of a healthy 45-year -old. Each value is given with their lower and upper bound.

	Lower	Upper	Unit	
R	2.525	3.495	mm	[12]
h	0.8875	1.3725	mm	[13]
E	236	1306	kPa	[9]
ν	0.4908	0.4912	-	[14]
ρ	1043	1054	$\mathrm{kg/m^3}$	[15]
μ	3.784	5.516	mPa s	[16]
R_{tot}	1.9066	2.3302	10^9 Pa s/$\mathrm{m^3}$	[17]
C	1.2192	1.4901	$10^{-10}\mathrm{m^3/Pa}$	[17]

accuracy of pressure, flow rate, and radius change values. Therefore, the maximal allowed time step $\Delta t_{\max}$ was used for the simulations.

2.3. Validation of the 1D model

As a first step of the validation process, we conducted UQSA of the 1D-model based on population variations in parameter values. The results of SA motivated us to place special focus on the structural mechanics of the FSI-solver. Therefore, we compared a finite element (FE) inflation test with the analytical solution of thin- and thick-walled cylinder theory.

Uncertainty quantification and sensitivity analysis

Measurement errors and lack of knowledge lead to uncertainties about model inputs and and thus propagate through numerical models to contribute to uncertainty about model outputs [18]. Quantifying this uncertainty is an integral part of the model verification and validation process [11], as well as a prerequisite for its implementation in clinical decision support [18]. However, computational costs for UQ increase with increasing number of uncertain model parameters and model dimension, limiting efficient analysis to low-fidelity models. This motivates to conduct UQSA on the 1D-model prior to its validation against the 3D-FSI model since UQSA will give insights into the model characteristics. Validation test cases can then be designed in such a way to capture these characteristics [11].

We considered a total of eight uncertain parameters based on the variations in a 45-year old healthy population given in literature. A uniform distribution was assumed for all parameters, summarized with their lower and upper bounds in Tab. 1. Due to lack of data and lack of knowledge, the uncertainty of the Windkessel model parameters, C and $R_{tot} = R + Z$, were assumed with a deviation of $\pm\,10\%$ from their respective reference value. Compliance was adjusted from reference values in order to represent a 45-year old subject, whereas vascular resistance was considered to be age-independent [17, 19]. The vessel length was held constant at $126\,\mathrm{mm}$ for UQSA. The 1D-model's governing equations can be summarized with the deterministic inputs $\mathbf{z}$ and deterministic output y with a black box functional f as

$$y = f(\mathbf{z}). \tag{7}$$

If model input parameters are uncertain, then the model output becomes uncertain as well. This is emphasized by rewriting Eq. 7 in terms of a stochastic vector of input variables, $\mathbf{Z}$, that yields a stochastic output Y

$$Y = f(\mathbf{Z}). \tag{8}$$

PC expansion was used for estimating uncertainty and sensitivity measures of this stochastic model, which can be written in the form of Eq. 8. A finite number of polynomials N approximate Y through a sum of expansion coefficients c_p and orthogonal polynomials Φ_p

$$Y \approx \sum_{p=0}^{N} c_p\ \Phi_p(\boldsymbol{Z}), \tag{9}$$

where the orthogonality of Φ_p is with respect to the distributions in $\mathbf{Z}$ [6].

SA attributes model output variance to particular model inputs, as well as to the interactions between the uncertain input parameters [4]. From the PC expansion, total variance of the model output, $\mathrm{Var}[Y]$, was computed as

$$\mathrm{Var}[Y] \approx \mathrm{Var}[Y_{PC}] = \sum_{p} \mathrm{Var}[c_p\ \Phi_p(\boldsymbol{Z})]. \tag{10}$$

The main sensitivity index S_i quantifies the direct effect of particular input parameter z_i on $\mathrm{Var}[Y]$. With the set A_i containing all basis functions depending only on z_i, the main sensitivity index S_i describing the fraction of output variance due to z_i, can be approximated as

$$S_i \approx \frac{1}{Var[Y_{PC}]} \sum_{p \in A_i} Var[c_p\ \Phi_p]. \tag{11}$$

The set $A_{T,i}$ contains all basis functions where the random input z_i and all its interactions with $z_{\sim i}$ are involved, such that the total model output variance with respect to z_i can be represented with the total sensitivity index ST_i as

$$ST_i \approx \frac{1}{Var[Y_{PC}]} \sum_{p \in A_{T,i}} Var[c_p\ \Phi_p]. \tag{12}$$

PC expansion of orders one to three were tested, showing that the sensitivity indices were already converged for the third order. At the mid-point of the vessel, we computed the sensitivity indices through time-averaging and weighting by the last cardiac cycle's variance, as well as normalizing with the model output variance [21].

3D-model formulation

The CCA is modelled as an idealized, hollow cylinder. Tab. 2 summarizes the dimensions and material properties of the model. The mathematical formulation of the 3D problem assumes an incompressible Newtonian fluid and a linear elastic vessel wall. Mass and momentum conservation of the fluid domain Ω_f are

$$\nabla \cdot \boldsymbol{u} = 0 \qquad \text{in } \Omega_f \tag{13a}$$

$$\rho_f \frac{\partial \boldsymbol{u}}{\partial t} + \rho_f \boldsymbol{u} \cdot \nabla \boldsymbol{u} = -\nabla p + \nabla \cdot \boldsymbol{\tau}_f + \boldsymbol{b} \quad \text{in } \Omega_f \tag{13b}$$

Table 2: Material parameters and dimensions of the 3D-FSI model. Material parameters, ρ_s, ρ_f, μ, and ν, are taken from [20].

Property	Value	Unit
Length L	115	mm
Unstressed radius R_d	2	mm
Wall thickness h	0.5	mm
Young's modulus E	700.0	kPa
Wall density ρ_s	1120	$\mathrm{kg/m^3}$
Wall Poisson ratio ν	0.49	-
Fluid density ρ_f	998.2	$\mathrm{kg/m^3}$
Fluid dynamic viscosity μ	1.003	mPa s

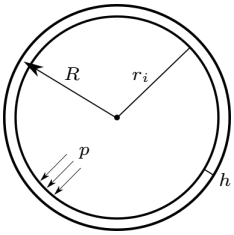

Figure 2: Representation of a thick-walled cylinder subjected to internal pressure p and external pressure $p_{ext} = 0$ Pa.

where ρ_f denotes the fluid density, $\boldsymbol{u}$, the fluid velocity, p the pressure inside the vessel, $\boldsymbol{\tau}_f = \mu_f(\nabla \boldsymbol{u} + (\nabla \boldsymbol{u})^T)$ the viscous stress tensor for a Newtonian fluid, and $\boldsymbol{b}$ body forces which are assumed to be zero. At the fluid-structure interface, a no-slip boundary condition was applied. The governing equations for the solid domain Ω_s are

$$\rho_s \frac{\partial \boldsymbol{u}_s}{\partial t} - \nabla \cdot \boldsymbol{\sigma}_s = \boldsymbol{b}_s \qquad \text{in } \Omega_s \quad (14a)$$

$$\boldsymbol{\sigma}_s \cdot \boldsymbol{n}_s = (-P\boldsymbol{I} + \boldsymbol{\tau}_f) \cdot \boldsymbol{n}_s \qquad \text{on } \Gamma \quad (14b)$$

with the wall density ρ_s, Cauchy stress tensor σ_s, body forces on the solid domain $\boldsymbol{b}_s$, which are assumed to be zero, and the outward normal vector $\boldsymbol{n}_s$ on Γ.

Static and transient inflation test
In order to assure the correct settings for the comparison between the 3D-FSI and the 1D-model, we tested the mechanical solver individually with a static and transient inflation test. Longitudinal displacement at the ends was either prohibited or allowed, representing thick-walled cylinder theory with fixed surfaces at the end or free surfaces without stress, respectively. Radial displacement was allowed in both cases. The pressure inside the tube was increased linearly from the reference pressure $p_0 = 0$ Pa to 20000 Pa over ten seconds. Large deformation of the domain was suppressed.
The wall displacement of the inflation test cases was compared with the analytical solution of the thick-walled cylinder theory, represented in Fig. 2. For a thick-walled cylinder with fixed ends and no external pressure acting on the outer surface is radial displacement described as [22]

$$u(R) = \frac{1}{2G} \frac{r_i}{1 - \left(\frac{r_i}{r_i+h}\right)^2} \left(\frac{r_i}{R} + (1-2\nu) \left(\frac{r_i}{r_i+h} \right)^2 \frac{R}{r_i} \right) P, \quad (15)$$

where r_i is the inner radius and G the shear modulus as

$$G = \frac{E}{2(1+\nu)}. \quad (16)$$

In order to represent the thick-walled cylinder with free ends, a correction term $\Delta u(R)$ needs to be added to Eq. 15

$$\Delta u(R) = -\frac{\nu^2}{G(1+\nu)} \frac{-(\frac{r_i}{r_i+h})^2 P}{1-(r_i+h)^2} R. \quad (17)$$

To investigate inertia effects, we tested simulation times of five seconds while maintaining the maximum pressure. This set of test cases resulted in a total of two static and four transient simulations. Mesh independence was demonstrated through three mesh refinements. All simulations were performed in Ansys Mechanical (Version 2021 R2) with the standard solver MAPDL. Time integration was performed with an implicit scheme.
In addition to the analytic thick-walled cylinder theory, the radial displacement was analysed under the assumption of a thin-walled cylinder with free ends. This analysis was conducted because the current 1D-model contains this assumption. The circumferential stress σ_c in a thin-walled cylinder [22] is

$$\sigma_c = \frac{P\,r}{h}, \quad (18)$$

with the middle radius $r = r_i + 0.5h$, where r_i is the inner vessel radius and h the vessel wall thickness. From the linear stress-strain relation it follows for the displacement

$$u_{thin} = \frac{P\,r^2}{E\,h}. \quad (19)$$

One-way FSI simulation without flow
To ensure a correct coupling between the fluid and the solid domain in the study, we conducted a one-way FSI simulation with the same pressure increase as in the inflation test, fixed ends of the artery, and a resting fluid domain. Ansys (Version 2020 R2) Fluent was used to generate and solve the fluid domain. Both solid and fluid domains consisted of hexahedral elements. A coupled pressure-velocity solver evaluated the fluid problem, and the standard MAPDL solver evaluated the solid problem. Since Ansys uses the segregated approach to solve a FSI problem, the equations are not solved simultaneously within one matrix [20]. Instead, each of the participant programs calculates its own problem. Fluent first iterates the fluid domain for a set number of iterations, then passes the evaluated force which the fluid exerts on the structure to Mechanical so that the displacement of the structural part can be obtained. This constitutes to one coupling iteration in one-way FSI simulations. One coupling step is equivalent to one time step and it contains a set number of coupling iterations. Ansys guidelines suggest between one and five. The number of iterations in Fluent was set to seven, Mechanical's iteration number was program controlled. The maximum amount of coupling iterations was five, with three usually being sufficient to meet the convergence criteria after a few time steps had passed since the start of the simulation [20].

3. Results

In Fig. 3, the time-averaged main and total sensitivity indices for the pressure, flow rate, and radius change predicted by the 1D-model, Eqs. 1-3, are presented for the mid-point of the artery. Further, the numerical values of the time-averaged main and total sensitivity indices for the qunatities of interest are given in Tab. 3. For all quantities of interest, the uncertainty in the Young's modulus is responsible for the largest part of the model output variation. Lumen radius and wall thickness have a minor influence, whereas the fluid properties ρ_f and μ, the Poisson ratio, and the total resistance of the Windkeseel model have no influence on model output variation. Additionally, all quantities of interest are slightly sensitive to the compliance value of the Windkessel model. For all uncertain input parameters the main and total sensitivity indices are approximately the same, indicating that parameter interaction does not play a significant role.
Over one cardiac cycle, Fig. 4 displays the 95 % prediction interval for the pressure and the relative radial

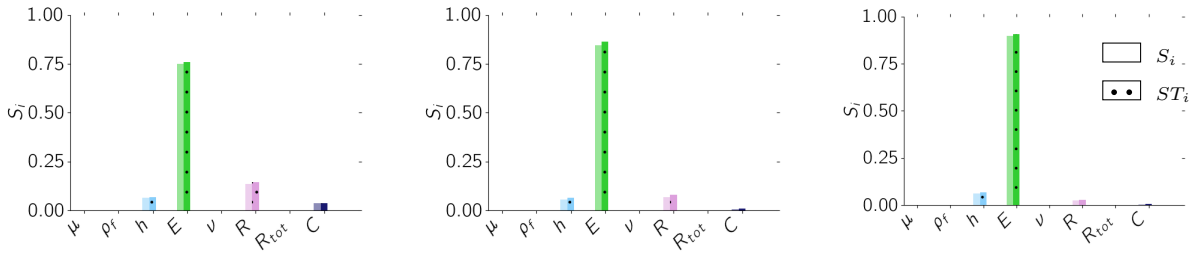

(a) (b) (c)

Figure 3: Main and total sensitivity indices, S_i and ST_i, respectively, evaluated at the mid-point of the 1D-model. All sensitivity indices are time-averaged over the last cardiac cycle. The quantities of interest are **(a)** pressure p, **(b)** flow rate Q, and **(c)** radius change ΔR with reference to the minimum radius of the respective model evaluation.

Table 3: Numerical values for the main and total sensitivity indices, S_i and ST_i, respectively, evaluated at the mid-point of the 1D-model for pressure p, flow rate Q, and radius change ΔR with reference to the minimum radius of the respective model evaluation. All sensitivity indices are time-averaged over the last cardiac cycle.

	μ		ρ_f		h		E		ν		R		R_{tot}		C	
	S	ST	S	ST	S	ST	S	ST	S	ST	S	ST	S	ST	S	ST
p	0.00	0.00	0.00	0.00	0.06	0.07	0.75	0.76	0.00	0.00	0.14	0.14	0.00	0.00	0.04	0.04
Q	0.00	0.00	0.00	0.00	0.06	0.07	0.85	0.86	0.00	0.00	0.07	0.08	0.00	0.00	0.01	0.01
ΔR	0.00	0.00	0.00	0.00	0.06	0.06	0.90	0.91	0.00	0.00	0.03	0.03	0.00	0.00	0.01	0.01

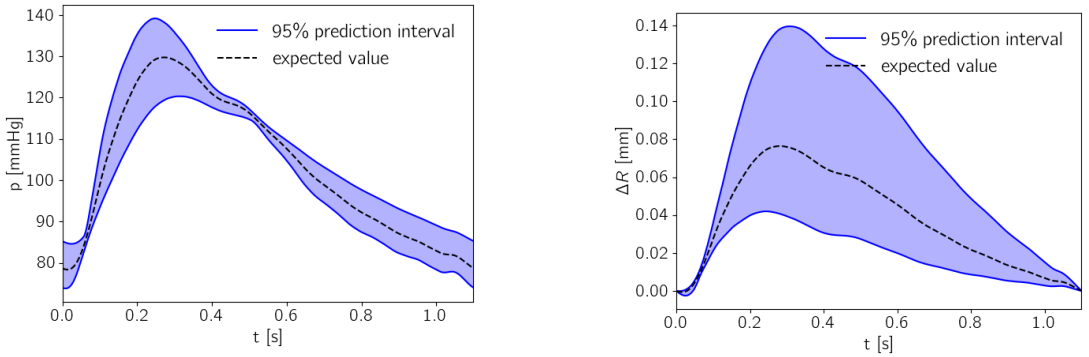

(a) (b)

Figure 4: 95% prediction interval for the last cardiac cycle at the mid point of the artery for the **(a)** pressure p and the **(b)** relative radius change ΔR with reference to the minimum radius of the respective model evaluation.

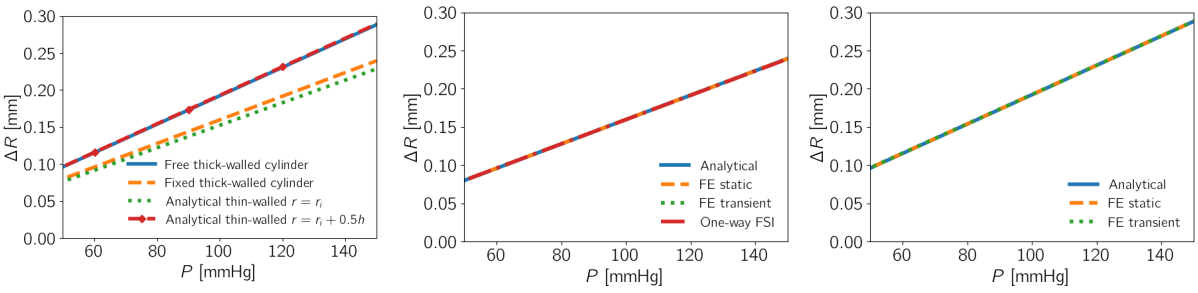

(a) (b) (c)

Figure 5: Comparison of analytical solutions of thin- and thick-walled cylinders with static and transient FE and one-way FSI inflation test. **(a)** analytical solutions with different underlying assumptions, **(b)** solution comparison with the assumption of fixed ends, and **(c)** solution comparison with the assumption of free ends.

displacement with reference to the minimum radius of the respective model evaluation predicted by the 1D-model at the mid-point of the artery. During early systole and around the dicrotic notch is the prediction band for the pressure very close to the expected pressure values. The relative radial displacement shows large variations at peak systole.

Results from the comparison of the inflation tests with analytical solutions for thick- and thin-walled cylinders are presented in Fig. 5. In our analysis, static and transient inflation tests for the 3D-FE model of the artery coincide with the analytical solution for a cylinder with fixed and free ends. The radial displacement of the one-way FSI-simulation with fixed ends agrees with the analytical and FE solution. Fig. 5a depicts the analytical solutions visualizing the underlying assumption on the radial displacement ΔR. For a thick-walled cylinder with free ends, ΔR is higher than for a thick-walled cylinder with fixed ends. For the thin-walled simplification, Eq. 19, using the internal lumen radius results in the largest discrepancy between 1D and 3D; however, using the mid-wall radius results in a near agreement with the thick-walled theory and 3D results.

4. Summary and Discussions

In this work, we verified that the simulations of a 1D arterial model were grid independent. Subsequently, UQSA of the 1D arterial model was performed using PC expansion. This UQSA served a role in the validation process to focus on comparison of the 1D wall model, Eq. 3, with results from the 3D-FSI model. To this end, we verified the solution during inflation of the 3D-FSI model against thick-walled cylinder theory and evaluated the 1D arterial model predictions against the 3D-FSI model of the CCA.

The SA suggests that the most sensitive input parameters are related to the arterial wall mechanics, namely the wall thickness h, the Young's modulus E, and the lumen radius R. Small sensitivity indices were estimated for the compliance C which might be due to the relation of the downstream vasculature's compliance to arterial wall properties. Since variations in the fluid properties, the Poisson ratio, and the total resistance do not lead to variations in the quantities of interest, this result suggests that these parameters can be set to average population values in further simulations. This reduces the number of parameters which need to be explored and with this decrease computational expenses as well.

The SA findings motivated a detailed analysis of the structural part of the FSI-model. We showed agreement between the analytical thick-walled cylinder theory and the FE inflation tests indicating that the boundary conditions and material properties were set correctly in the simulation. Since the transient and static simulation results coincided, the inflation tests were not influenced by inertia effects. Furthermore, the consensus between the FSI simulation and the analytical solution assure correct coupling between the fluid and the solid domain.

The discrepancy between the analytical thin- and thick-walled cylinder with fixed ends radial displacement under internal pressure indicates that the wall model in the current 1D-model needs to be revised in order to lead to the same displacement as the 3D-FSI model.

5. Conclusions

With this work we showed that UQSA during the validation process can elucidate model characteristics where specific emphasis needs to be placed on during the validation process. In our specific case, special focus needs to be placed on the wall mechanics because variations in the arterial wall input parameters lead to the largest variations in the model output.

In a next step, the FSI inflation test will be simulated with a two-way coupling and the 1D wall model will be advanced such that the average cylinder radius in the thin-walled theory is used for the computation instead of the inner radius. After successful completion, a physiological flow rate and pressure wave will be applied at the boundaries of the 3D-FSI model as well as at the 1D-model. The discrepancy between the model predictions will be quantified closing the validation process.

Acknowledgment

The authors would like to thank the Polish National Science Center GRIEG programme, (Grant no: UMO-2019/34/H/ST8/00624) for providing financial support to this project.

References

[1] M. F. O'Rourke, C. O'Brien, and T. Weber, "Arterial stiffness, wave reflection, wave amplification: Basic concepts, principles of measurement and analysis in humans," in *Blood Pressure and Arterial Wall Mechanics in Cardiovascular Diseases* (M. E. Safar, M. F. O'Rourke, and E. D. Frohlich, eds.), pp. 3–13, Springer, 2014.

[2] P. M. Nabeel, V. R. Kiran, J. Joseph, V. V. Abhidev, and M. Sivaprakasam, "Local pulse wave velocity: Theory, methods, advancements, and clinical applications," *IEEE Reviews in Biomedical Engineering*, vol. 13, pp. 74–112, 2020. Conference Name: IEEE Reviews in Biomedical Engineering.

[3] J. Alastruey, A. W. Khir, K. S. Matthys, P. Segers, S. J. Sherwin, P. R. Verdonck, K. H. Parker, and J. Peiró, "Pulse wave propagation in a model human arterial network: Assessment of 1-d visco-elastic simulations against in vitro measurements," *Journal of Biomechanics*, vol. 44, no. 12, pp. 2250–2258, 2011.

[4] A. Saltelli, M. Ratto, T. Andres, F. Campolongo, J. Cariboni, D. Gatelli, M. Saisana, and S. Tarantola, *Global sensitivity analysis the primer*. John Wiley, 2008.

[5] G. Ninos, V. Bartzis, N. Merlemis, and I. E. Sarris, "Uncertainty quantification implementations in human hemodynamic flows," *Computer Methods and Programs in Biomedicine*, vol. 203, p. 106021, 2021.

[6] V. G. Eck, W. P. Donders, J. Sturdy, J. Feinberg, T. Delhaas, L. R. Hellevik, and W. Huberts, "A guide to uncertainty quantification and sensitivity analysis for cardiovascular applications," *International Journal for Numerical Methods in Biomedical Engineering*, vol. 32, no. 8, p. e02755, 2016.

[7] S. Sherwin, V. Franke, J. Peiró, and K. Parker, "One-dimensional modelling of a vascular network in space-time variables," *Journal of Engineering Mathematics*, vol. 47, no. 3, pp. 217–250, 2003.

[8] C. A. Figueroa, I. E. Vignon-Clementel, K. E. Jansen, T. J. Hughes, and C. A. Taylor, "A coupled momentum method for modeling blood flow in three-dimensional deformable arteries," *Computer Methods in Applied Mechanics and Engineering*, vol. 195, no. 41, pp. 5685–5706, 2006.

[9] W. A. Riley, R. W. Barnes, G. W. Evans, and G. L. Burke, "Ultrasonic measurement of the elastic modulus of the common carotid artery. the atherosclerosis risk in communities (ARIC) study.," *Stroke*, vol. 23, no. 7, pp. 952–956, 1992.

[10] L. Formaggia, D. Lamponi, and A. Quarteroni, "One-dimensional models for blood flow in arteries," p. 26, 2003.

[11] A. E. Anderson, B. J. Ellis, and J. A. Weiss, "Verification, validation and sensitivity studies in computational

biomechanics," *Computer Methods in Biomechanics and Biomedical Engineering*, vol. 10, no. 3, pp. 171–184, 2007.

[12] C. Sass, B. Herbeth, O. Chapet, G. Siest, S. Visvikis, and F. Zannad, "Intima–media thickness and diameter of carotid and femoral arteries in children, adolescents and adults from the stanislas cohort: effect of age, sex, anthropometry and blood pressure," *J Hypertens*, vol. 16, no. 11, pp. 1593–1602, 1998. Place: Hagerstown, MD Publisher: Hagerstown, MD: Lippincott Williams & Wilkins, Inc.

[13] M. R. Skilton, L. Boussel, F. Bonnet, S. Bernard, P. C. Douek, P. Moulin, and A. Serusclat, "Carotid intima–media and adventitial thickening: Comparison of new and established ultrasound and magnetic resonance imaging techniques," *Atherosclerosis*, vol. 215, no. 2, pp. 405–410, 2011.

[14] A. Karimi, T. Sera, S. Kudo, and M. Navidbakhsh, "Experimental verification of the healthy and atherosclerotic coronary arteries incompressibility via digital image correlation," *Artery Research*, vol. 16, p. 1, 2016.

[15] T. Kenner, "The measurement of blood density and its meaning," *Basic Research in Cardiology*, vol. 84, no. 2, pp. 111–124, 1989.

[16] C. Irace, C. Carallo, F. Scavelli, T. Esposito, M. S. De Franceschi, C. Tripolino, and A. Gnasso, "Influence of blood lipids on plasma and blood viscosity," *Clinical Hemorheology & Microcirculation*, vol. 57, no. 3, pp. 283–290, 2014. Publisher: IOS Press.

[17] N. Xiao, J. Alastruey, and C. A. Figueroa, "A systematic comparison between 1-d and 3-d hemodynamics in compliant arterial models," *International Journal for Numerical Methods in Biomedical Engineering*, vol. 30, no. 2, pp. 204–231, 2014. _eprint: https://onlinelibrary.wiley.com/doi/pdf/10.1002/cnm.2598.

[18] W. Huberts, S. G. Heinen, N. Zonnebeld, D. A. van den Heuvel, J.-P. P. de Vries, J. H. Tordoir, D. R. Hose, T. Delhaas, and F. N. van de Vosse, "What is needed to make cardiovascular models suitable for clinical decision support? a viewpoint paper," *Journal of Computational Science*, vol. 24, pp. 68–84, 2018.

[19] P. H. Charlton, J. Mariscal Harana, S. Vennin, Y. Li, P. Chowienczyk, and J. Alastruey, "Modeling arterial pulse waves in healthy aging: a database for in silico evaluation of hemodynamics and pulse wave indexes," *American Journal of Physiology-Heart and Circulatory Physiology*, vol. 317, no. 5, pp. H1062–H1085, 2019.

[20] A. Inc., "Ansys FSI lecture trainee." 2021.

[21] V. Eck, J. Sturdy, and L. Hellevik, "Effects of arterial wall models and measurement uncertainties on cardiovascular model predictions," *Journal of Biomechanics*, vol. 50, pp. 188–194, 2017.

[22] F. Irgens, *Continuum mechanics*. Springer, 2008.